

PAPER • OPEN ACCESS

## Hingeless arm for space robotics actuated through shape memory alloys

To cite this article: Tiziana Biasutti *et al* 2024 *Bioinspir. Biomim.* **19** 016011

View the [article online](#) for updates and enhancements.

You may also like

- [A novel active fire protection approach for structural steel members using NiTi shape memory alloy](#)  
H Sadiq, M B Wong, R Al-Mahaidi et al.
- [A review of modeling techniques for advanced effects in shape memory alloy behavior](#)  
Cheikh Cisse, Wael Zaki and Tarak Ben Zineb
- [Study of pseudoelastic systems for the design of complex passive dampers: static analysis and modeling](#)  
Adelaide Nespoli, Daniela Rigamonti, Marco Riva et al.

# Bioinspiration & Biomimetics



## PAPER

# Hingeless arm for space robotics actuated through shape memory alloys


### OPEN ACCESS

RECEIVED  
5 August 2022

REVISED  
28 July 2023

ACCEPTED FOR PUBLICATION  
28 November 2023

PUBLISHED  
18 December 2023

Tiziana Biasutti, Daniela Rigamonti\* , Emanuele Casciari, Antonio Mattia Grande  and Paolo Bettini

Dipartimento di Scienze e Tecnologie Aerospaziali, Politecnico di Milano, Milan, Italy

\* Author to whom any correspondence should be addressed.

E-mail: [daniela.rigamonti@polimi.it](mailto:daniela.rigamonti@polimi.it)

**Keywords:** shape memory alloys, NiTiNOL, continuous structures, composite materials, minimum weight, flexibility

Original content from this work may be used under the terms of the [Creative Commons Attribution 4.0 licence](https://creativecommons.org/licenses/by/4.0/).

Any further distribution of this work must maintain attribution to the author(s) and the title of the work, journal citation and DOI.



## Abstract

Operating outside the spacecraft via remotely controlled structures is an important opportunity in different space applications. The research in this area is focused on designing robots that are sufficiently flexible to allow inspection in locations where access is difficult or impossible for astronauts, while minimizing weight and bulk. The purpose of the research is to design a borescope for space applications with no hinges or other mechanisms, exploiting biomimetic design concepts. This is pursued by giving to the borescope a backbone exoskeleton provided by a continuous structure made of fibre reinforced composite material and using NiTi wires as tendons, taking advantage of their low weight and dimensions, which allow them to be embedded between the composite layers during the lamination process. After a study of the state of the art of flexible structures, concentrated in the medical and robotic fields, the research work unfolded in two phases. In the first design phase, several composite layup solutions were considered and analysed using finite element models, leading to the definition of the borescope geometrical parameters and to an initial estimate of the displacements that can be achieved. In the second experimental phase, seven prototypes were produced and tested, with one or more wires, to validate the design and to search for a configuration that can be actuated in different directions. The borescope prototypes resulted flexible enough to achieve an extended degree of bending and at the same time sufficiently rigid to allow complete rearm of the NiTi wires. The numerical and experimental study led to the definition of the design parameters, the number of wires, and the manufacturing technique to integrate NiTi actuators.

## 1. Introduction





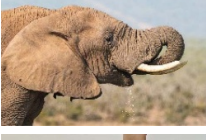


Robotics and automation are among the most studied areas of engineering research in recent decades. Designing machines controlled remotely is advantageous, especially in areas where human access can be complex due to limited space or dangerous working conditions, like, e.g. in biomedical and space fields. Delicate surgery with low invasiveness in patients is possible with tools designed for specific procedures that can reduce the recovery time [1, 2]. In space, on the other hand, access to the area outside the vehicle is complex and it is usually done through robots [3, 4].

Continuous jointless structures are particularly suitable for these applications because they are more flexible and reliable than common robots, due to

lack of complex mechanisms, and have almost infinite degrees of freedom [5]; furthermore, they are lighter and potentially more precise. However, they frequently can present non-linear behaviour.

The design of these structures is often inspired by animal and vegetal world and the employed materials can take advantage of bio-mimetic principle as well. Some flexible materials acting as animal skin or plant membranes are polymers such as polyamide or silicone. Metallic alloys (e.g. aluminium and titanium based ones) often play the role of stiff constituent for support structures same as the skeleton. Smart materials, like shape memory alloys (SMAs), act as muscles and tendons. Kolachalama and Lakshmanan [6] have collected some of the most important examples of continuous bioinspired robots here reported in table 1.

Table 1. Examples of continuous bioinspired robots

Bio-inspiration	Model	Example of continuous robot
Snake		[2], Jeffrey Surianto/Pexels.com
Biological vine and plant		[4, 7], Ravi Kant/Pexels.com
Spine of a mammal		[5], Tima Miroshnichenko/Pexels.com
Octopus arm		[8, 9], Ashley Christiano/Pexels.com
Elephant trunk		[10, 11], Charl Durand/Pexels.com
Human arm and fingers		[12], Daria Liudnaya/Pexels.com
Tongue and tail of a reptile		[13], Yuvi's picworld/Pexels.com

The actuation of these robots is usually obtained through pneumatic or electrical motors. The former have the advantages of being less complex and cheaper, so they are usually employed in continuous robots. The latter are mainly used for tendon-driven continuous robots and they can be divided into motors actuated with direct current [4, 7], servo electric motors [8], and steppers. These actuations usually are bulky and heavy. These two characteristics represent a big limit, especially for space applications. Some of the most famous continuous robots that used these materials are octopus limbs [9] and elephant trunks [10, 11].

A possible solution for the actuation of simple systems is the use of SMAs, like NiTiNOL (NiTi). NiTi is generally manufactured in the shape of wires, plates, and springs. The elongated geometries exploit the shape memory capability by establishing a preferential direction of action in which the recovery is maximized. The small volume makes these actuators easily embedded inside the systems. Their main advantages as actuators are high force vs dimensions ratio and corrosion resistance. On the other end, their

activation time is not negligible and can limit their range of applicability. If a subsequent activation cycle is required, the material must be cooled to rearm the actuator before a new activation can take place. A lot of studies evaluated the adoption of devoted cooling methods to reduce activation times [14]. A characteristic time in the range between 0.3 and 1 s was reached by using a heat sink method to cool NiTi wires with 0.2 mm of diameter [15].

SMA as actuators are mainly applied in biomedical applications, taking advantage of the biocompatibility of the NiTi and their small dimension and lightness [16], but they are also widely studied in other areas such as civil [17] and aerospace engineering [18].

Some examples of medical structures actuated with NiTi are endoscopes with two or more degrees of freedom [19, 20], active catheters [21–23], and intestinal tubes [24]. These structures have small dimensions and the region that is actuated is only a portion of the total length, usually the terminal part of the arm. Moreover, the structure usually includes hinges bonded through NiTi wires or springs [25, 26].

The active endoscope developed in [20] by De Sars is a 320 mm long tube composed of six stainless steel rings with an external diameter of 7 mm. The actuation was performed by two pairs of antagonists' wires disposed at  $90^\circ$ . In this research different initial strains of NiTi wires were studied in the range of 1%–7% to find the optimal solution concerning the stiffness of the structure. The maximal bending angle reached was  $100^\circ$  and the curvature radius was 90 mm. This configuration with different sections in stainless steel linked by NiTi wires is proposed by different works. In [19] Fisher developed a flexible distal tip for medical applications. The flexible part of the structure has a diameter of 10.5 mm and a length of 25.6 mm. Also in this case the structure is composed of different rings in stainless steel actuated by wires. This solution allows reaching angles in the range of  $0^\circ$ – $90^\circ$ .

Haga *et al* [21], compared to previous research works, designed an active catheter that reproduces also torsional movements. The structure is composed of joints actuated individually. The external diameter is 1.4 mm. Three SMA springs are fixed coaxially inside a linear coil and allow the torque of the structure, reaching angles of  $70^\circ$  with a current of 80 mA. Another active guide with an external bias coil in stainless steel with a diameter of 0.5 mm was developed by Mineta [22]. This configuration allowed bending in one direction, reaching angles of  $60^\circ$ . After the actuation the structure did not restore the initial position, the residual angle was always  $20^\circ$ . Haga *et al* [23] also developed an ileus tube for intestinal obstructions actuated in one direction by micro coils. The tube was 40 mm long and had an external diameter of 5 mm. The structure was composed by six sections connected by the NiTiNOL coils. The maximum angle reached with this solution was  $110^\circ$ , and the corresponding radius of curvature was 20 mm.

In [27] the aim of Padasdao was the development of an entirely NiTiNOL structure with notches of different shapes and dimensions and two NiTi wires tendons. The prototype could recover high deformations through pseudoelastic effect, while the two tendons used the shape memory effect for the actuation. The tube was 11.25 mm long and had an external diameter of 2 mm. Numerically the displacement of the tube was estimated at  $37^\circ$  in both directions, left and right. Experimentally the angles reached were  $28.33^\circ$  in one direction and  $19.72^\circ$  in the other. A similar structure was also proposed by Sarma *et al* [28]. The support structure manufactured in NiTiNOL is a recurring solution that allows to recover high strain. For example also Tian *et al* [29] a NiTi spiral with different cutting patterns. In this case the actuation was not performed by SMA wires because the aim was to test the rigidity of the prototypes and understand their ability to deform. The angles range testes were  $0^\circ$ – $180^\circ$ .

Another medical device actuated through SMA was proposed by Sivaperuman Kalairaj *et al* [30] for sinus transnasal drug delivery. The structure was composed of a stainless steel ribbon spring with an external diameter of 2 mm and a length of 12 mm. A NiTiNOL wire actuated the ribbon spring, and the initial configuration was recovered by the strength of the spring. Controlling the voltage is possible to reach different bending angles. For voltage in the range of 1.2–2 V, the structure reaches angles between  $36.2^\circ$  and  $66.8^\circ$ .

These were some of the configurations taken into account for the development of a proof of concept for a structure activated by SMA intended for space applications. The architectures more relevant for our project are in stainless steel and actuated by usually 2–4 wires or springs. In the majority of the cases usually, also an external coating is present. Moreover, the section actuated is only a fraction of the complete structure. The dimensions viewed are small because we considered biomedical applications. The structures' angle of deflection range from  $20^\circ$  to  $110^\circ$ .

The project aims to design a self-sustaining continuous structure entirely actuated through NiTi wires and without hinges or other mechanisms. The selected material, to meet these requests, was a fibre reinforced composite material. This solution allows to choose the appropriate structure properties defining the lamination sequence. Moreover, composite materials are employed in space structures with good reliability. The continuity in the component is obtained through a spiral shape. This allows to have a prototype adequately rigid without an outer coating. In this phase of the research, only a preliminary study was performed, valuating the possible performance of the design realised. Further thermal and fatigue performance analyses are reserved to future research phases.

## 2. Methodologies

In this work, numerical simulations followed by experimental testing investigated the feasibility of a continuum composite structure activated by NiTi wires.

Initially, some simplified analyses were implemented in Abaqus to determine the optimal geometrical parameters. The composite material modelled was ET445 3KT300 2x2T will carbon fabric prepreg. In these initial analyses the interaction with the NiTi wires was not considered. Some geometrical parameters were previously fixed, whereas pitch, strip width and lamination sequence were varied.

After the helix design, the activation of the structure was studied. In this case were modelled also the NiTi wires (SmartFlex from Saes Getters with 0.2 mm diameter). For the implementation of SMA behaviour was used a user material (UMAT) subroutine.

This one reproduces the shape memory effect and the pseudoelastic effect of NiTi, depending on the temperature and the initial martensitic fraction given in input, using the Boyd and Lagoudas model [31, 32].

The experimental part consists of the preliminary design of a dedicated mould for the manufacturing and a suitable template made in polyamide to guide the lamination process. In this phase also the set up for the testing of the prototype was studied. Both the mould and the basement for the testing are in aluminium.

### 3. Design and numerical simulations

#### 3.1. Composite helix geometry design

The first aspect defined was the geometry of the slender backbone. A helix structure equipped with wires inserted along the generators was the most convenient. This solution results from a trade-off between the actuation in different directions and the future manufacturing procedure. The structure allows embedding NiTi wires in each turn of the helix along the circumference.

Some of the geometrical parameters were fixed initially: helix length at 500 mm and diameter at 10 mm. For the other parameters, numerical optimization analyses were performed by varying the pitch of the helix and the width of the strip. For the selection of parameters' range the subsequent difficulties of cutting small patches of composite and managing small plies during the lamination process were considered. Concerning these furthermore, the choice of a fabric composite was the best solution. Two different lamination sequences were considered: a first homogeneous one with layup  $[0]_4$  and a second one introducing angled plies with layup  $[0/45/45/0]$ .

In the preliminary analysis, only the helix was numerically modelled. The wire behaviour was simulated by applying 10 N force couples in positive and negative directions, which reproduced the contraction of the wire when activated (figure 1). This choice was functional to the simplification of this preliminary model, whose purpose was only to obtain a comparison between the different configurations. The value of 10 N was a fair assumed value based on previous applications of the same type of NiTi wire.

#### 3.2. Helix actuation

A refined model with NiTi wires and composite structure was implemented considering the geometry obtained previously. Three different dispositions of wires were studied: one single wire, two wires at  $0^\circ$  and  $180^\circ$ , and six wires, homogeneously distributed along the circumference (with a spacing of  $60^\circ$ ). The reasons for these configurations will be explained in the manufacturing section. The NiTi wires were added only in the free portion between two turns of the composite helix since the contribution of the NiTi embedded inside the composite was considered

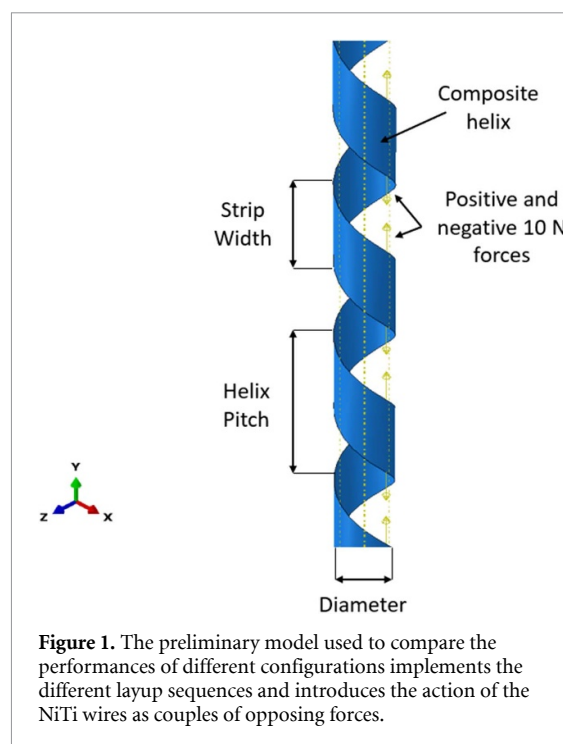


**Figure 1.** The preliminary model used to compare the performances of different configurations implements the different layup sequences and introduces the action of the NiTi wires as couples of opposing forces.

negligible concerning the total displacement of the structure. They were modelled using beam elements, while the composite structure was modelled with shell elements. The composite mechanical properties were valued by experimental traction tests.

For our purpose, the material was initially in a martensitic phase. The wire's mechanical and thermal properties are reported in table 2. They were provided by the supplier and controlled experimentally in previous activities.

The analysis is characterized by two steps. In the first step, an initial deformation of 4% was imposed on the NiTi wires. In the second step, the constraint between the wires and the structure was set and the actuation of the wires was simulated, increasing linearly the temperature of one single wire from room temperature to  $110^\circ\text{C}$ . The non-activated wires were considered only with their stiffness contribution, without the shape memory behaviour.

#### 3.3. Preliminary helix geometry design results

The best performances were obtained with 25 mm pitch, 10 mm width, and lamination sequence  $[0]_4$ . The results of the analyses are presented in table 3. As previously said, the variable used to evaluate the bending performance was the lateral displacement of the tip of the helix U1.

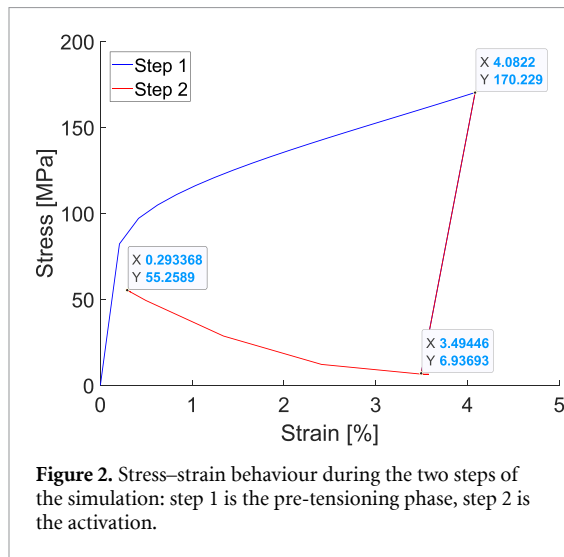
As expected, when the width of the strip was increased, the total displacement of the helix decreased considerably, due to the rise of the stiffness of the composite structure. Varying the pitch, the results obtained did not vary remarkably for the same width, showing that this parameter had a smaller influence than the previous in the final displacement. The lamination sequence had a high impact on the

**Table 2.** Mechanical and thermal parameters used to model SMA wires

Symbol	Description	Unit	Value
$x_{i0}$	Initial stress-induced only martensitic volume fraction	—	0
$E_A$	Young's modulus for austenite	GPa	40.24
$E_M$	Young's modulus for martensite	GPa	24.07
$\nu$	Poisson's ratio	—	0.33
$\alpha$	Thermal expansion coefficient (both A and M)	$1\text{ K}^{-1}$	$2.2 \times 10^{-5}$
$M_S$	Martensitic start temperature	K	286.97
$M_F$	Martensitic finish temperature	K	265.50
$A_S$	Austenitic start temperature	K	333.77
$A_F$	Austenitic finish temperature	K	348.26
H	Maximum transformation strain	—	0.052
$\left(\frac{\Delta\sigma}{\Delta T}\right)_M$	Martensitic Clausius–Clapeyron coefficient	$\text{MPa K}^{-1}$	5.036
$\left(\frac{\Delta\sigma}{\Delta T}\right)_A$	Austenitic Clausius–Clapeyron coefficient	$\text{MPa K}^{-1}$	7.210

**Table 3.** Comparison of the preliminary Helix geometry design results

Pitch (mm)	Width (mm)	Displacement U1 (mm)	
		$[0]_4$	$[0/45/45/0]$
25	10	273.4	155.9
	15	110.4	68.3
	20	51.2	33.8
30	10	273.7	151.7
	15	118.4	69.1
	20	56.2	34.7
	25	30.0	19.3



results. The best solution was with layers cut at  $0^\circ$ . This means that the fibres were not aligned in the bending direction. Indeed, when the composite was deposited for the manufacturing of the helix, the reference direction was one of the windings of the strip on the cylindrical envelope of the helix.

### 3.4. Results of the helix numerical actuation

The graph reported in figure 2 describes the stress and strain trends at the tip of the structure. The curve was characterized by two parts. The first part followed the stress–strain curve of martensitic material until

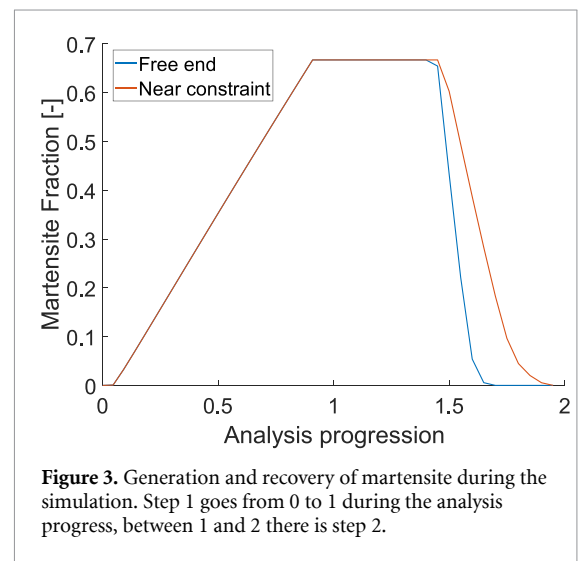


**Figure 3.** Generation and recovery of martensite during the simulation. Step 1 goes from 0 to 1 during the analysis progress, between 1 and 2 there is step 2.

the 4% deformation, the one imposed in the simulation during the pre-tensioning phase. The second part corresponded to the heating step. Here, the stress and strain initially decreased during the unloading of the structure, until the temperature overpassed the austenitic start one, so the wire starts the activation. When the recovery of the initial length of the wire started, the stress in the structure increased while the strain decreased. The residual strain in the wire was 0.3%, so the shape recovery was almost complete.

Figure 3 shows the martensitic fraction in the first and second steps at the constraint and the tip of the helix. In the first step, the strain was applied uniformly on every section of the wire. The martensitic fraction increased until most of the material started to orient in the load direction. In this step, there was the detwinning of the martensite. During the recovery, in the second step, the stresses in the tip region were lower and, consequently, the transformation temperatures were reduced as well. For these reasons, the decrease of the martensitic fraction was faster at the free end. The graph shows that the almost total recovery of the deformation ended early at the tip of the helix.

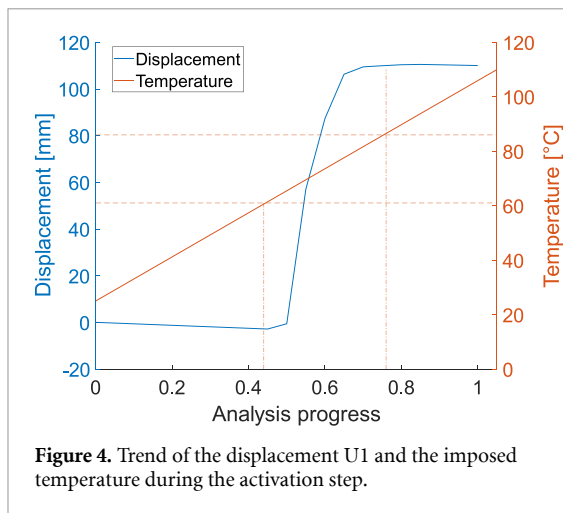


**Figure 4.** Trend of the displacement  $U_1$  and the imposed temperature during the activation step.

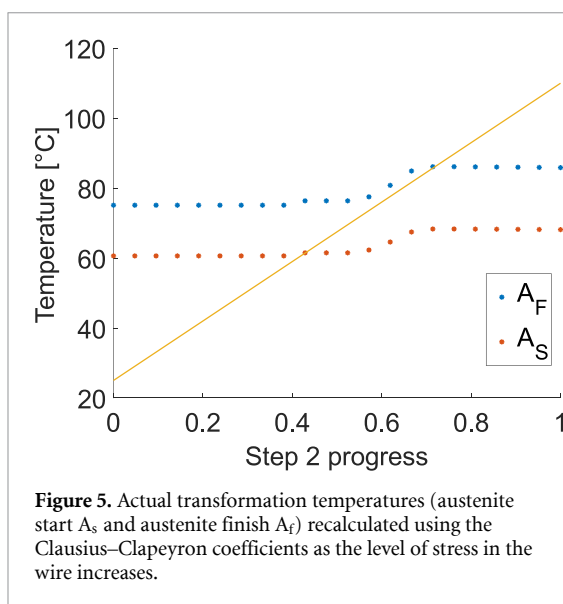


**Figure 5.** Actual transformation temperatures (austenite start  $A_s$  and austenite finish  $A_f$ ) recalculated using the Clausius–Clapeyron coefficients as the level of stress in the wire increases.

The displacement and the temperature increase in the second step are reported in figure 4. The structure starts to move when the temperature exceeds the Austenite Start temperature. When the wire reaches the austenite finish temperature, the displacement stabilizes at the final displacement of the structure.

The actual transformation temperatures, considering the stresses applied on the NiTi wire, were calculated using the Clausius–Clapeyron curve and reported in figure 5. The blue and red dotted lines represent the Austenite finish and start temperatures in the second step. Also, in this graph, a clear S-trend that represents the actuation of the wire is visible. The yellow line illustrates the linear increase of wire temperature imposed in the second step. The intersections of the three curves in figure 5 give the actual transformation temperatures, reported also in the displacement-temperature graph in figure 4 (vertical red lines).

In table 4, the results of the simulations with 1, 2, and 6 wires are reported. Increasing the number of wires, the stiffness of the structure increased.

Consequently, the total displacement and the percentage of strain recovered decreased. Moreover, the structure opposed a greater resistance to the NiTi actuation, so the final stresses were higher. This also influenced the transformation temperatures and the final displacement.

## 4. Experimental procedure and results

### 4.1. Manufacturing and testing methods

The structure was produced using ET445 3KT300 2x2T will carbon fabric prepreg. A helix template, manufactured in polyimide via 3D printing, was used to maintain the correct pitch and winding angle during the manual deposition of the layers. This template is the negative of our composite structure and only five turns of the helix were manufactured to facilitate the handling during the depositions of composite layers. Four layers were cut and overlaid with an orientation of  $0^\circ$ . The polyimide helix was used as a reference only for the first layer. The subsequent layers were laid down following the first one. The wires were embedded between the second and the third layer. Two configurations were considered. The first one is with a direct embedding of the NiTi wires between the composite layers. The second configuration, on the other hand, involved the use of Teflon sleeves between the layers. In this way, the wire is totally free to actuate, even if the invasiveness is higher [33]. The total length of the NiTiNOL wire was almost 800 mm. The complete composite structure consists of 22 turns, with a total length of 500 mm.

A specific mould made of aluminium (figure 6) was designed and manufactured to keep the wires positioned and tensioned during the autoclave cycle. The structure was symmetrical and composed of three parts: the central rod and two lateral fixtures. Each of the lateral fixtures was in turn the combination of two components: the inner one with six semi-holes for keeping the wires in position, and the second one in which the wires were fixed with bolts (figure 8). The lamination of the helix was performed in the central part of the rod (figure 7).

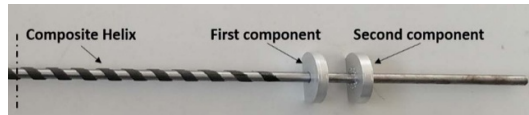
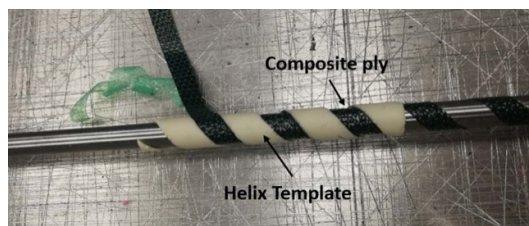
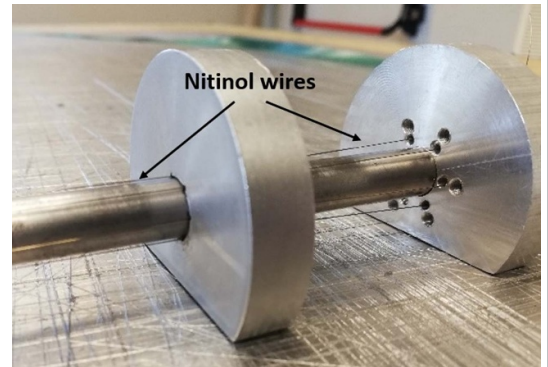
Different prototypes were manufactured with the characteristics reported in table 5. All the wires are provided with an initial strain of 3% and stabilized in this configuration. The 6% strain was reached by tensioning the wire before the embedding. This was done to observe the behaviour of the structure with a higher initial deformation.

The sleeves used in the second configuration were cut at suitable dimensions before the manufacturing, as shown in figure 9(b).

The reason for the variation in the number of wires is related to the choice to study different situation and find the optimal solution. The configuration with one wire was the initial one, to examine the

**Table 4.** Comparison of the results of the simulations with 1, 2, and 6 wires

	Final stress (MPa)	Final strain (%)	Strain recovery percentage	Displacement (mm)
1 wire	55.40	0.311	92.22	110
2 wires	74.26	0.315	92.12	101
6 wires	78.05	0.350	91.25	99

**Figure 6.** Mould in aluminium to manufacture the helix. The structure is symmetric. In figure is reported only half of mould.**Figure 7.** Polyimide helix used as track to produce the composite helix with embedded NiTi wires. The carbon reinforced composite strip can be noticed on the central cylinder.**Figure 8.** A detail of the lateral fixtures that allow keeping the wires positioned and tensioned during autoclave curing. The inner component positions the wires on the left side of the picture and the outer one to fix them on the right side.

technology and the set-up realize for the manufacturing. It is the simplest one and allows for verification of the feasibility of the prototype designed. The second configuration was one with two wires placed at opposite sites. This was done to slowly add complexity to the structure and to investigate how the presence of a passive wire influenced the behaviour of the one activated. Moreover, in these structures is possible to test the ability of the arm to come back to the initial position, eventually through the activation of the opposite wire. The third solution was the one with three wires; this is the situation where is possible to activate the structure in all directions with the minimum number of wires. And finally, the last configuration has six wires and in this case, is possible to reach a higher precision of movements. Moreover, it is possible to continue the analysis of the influence of passive wires during the activation.

A dedicated setup has been designed for the activation tests. Prototypes were fixed at one end in the vertical position and, according to the simulations, the lateral displacement of the point of the helix tip was measured while the wires were activated (figure 15).

The helical structure of the prototypes was held in place with an aluminium base plate, as visible in figure 10. Sixteen holes in the plate allow to close off the wires between each other and let them work without risky contacts that can cause short-circuit.

This structure was also designed to constrain prototypes with different geometric dimensions. The correct positioning was guaranteed by the possibility of moving the bolts on the plate.

During tests, the heating of the wire was obtained through the Joule effect. The tension applied on the extremities of the wire was 10 V, which corresponds to a current of about 1 A. The cooling was performed by natural convection, since this was a preliminary study.

The acquisition of displacement of the helix tip during the actuation was obtained by implementing a program that uses the Lucas–Kanade method on Visual Studio Code with the Python programming language. The Lucas–Kanade method [34], developed by Bruce D Lucas and Takeo Kanade, is a widely used differential method for estimating optical flow. It is assumed that the flow is essentially constant in a local neighbourhood of the pixel under consideration and solves the basic optical flux equations for all pixels in that area, with the criterion of least squares.

The frames to be analysed with the program were obtained by using two cameras positioned perpendicular to each other and elevated with respect to the workbench. One camera was placed in front of the prototype while the other was beside the structure, as visible in figure 11. The whole system was calibrated before the test session.

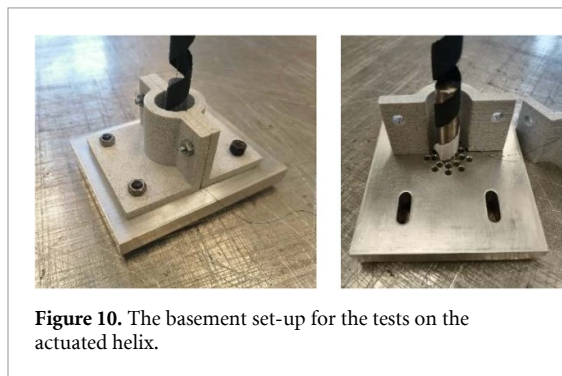
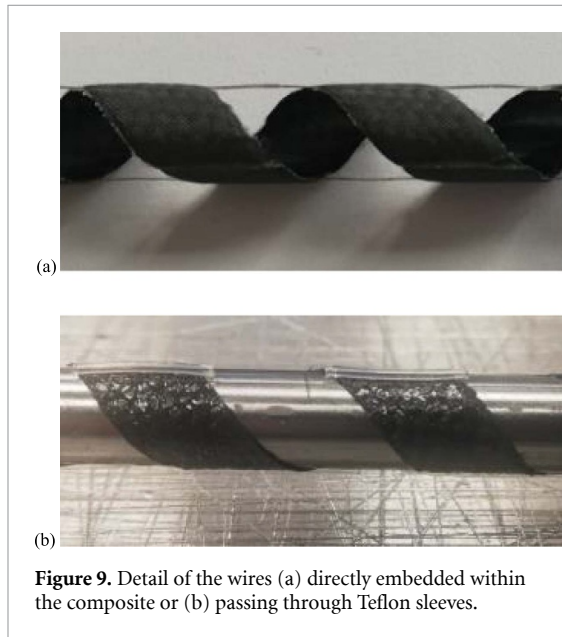
#### 4.2. Experimental results

The parameter detected by the cameras was the displacement of the tip of the helix during both the heating (actuation) and the cooling (recovery and rearm) of the structure. All the wires were activated singularly ten times. The wires were supplied already stabilized;



**Table 5.** Summary of the configuration of the manufactured prototypes

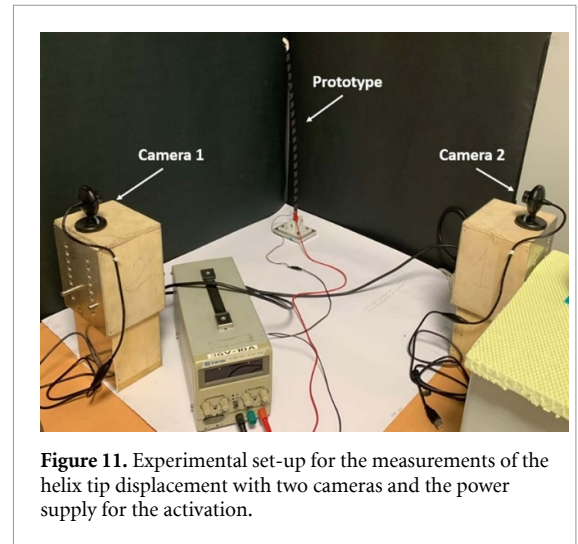
#Prototype	Description
1	Single wire, direct embedding, prestrain = 3%
2	Two wires, direct embedding, prestrain = 3%
3	Two wires, direct embedding, prestrain = 6%
4	Two wires, sleeves with extremity clamps, prestrain = 3%
5	Two wires, sleeves and direct embedding only in the last turn of the helix, prestrain = 3%
6	Three wires, sleeves and direct embedding only in the last turn of the helix, prestrain = 3%
7	Six wires, direct embedding, prestrain = 3%



the repeated actuation was done only to see the complete recovery of the structure and the repeatability of the movements. Table 6 reports the average maximum displacements for each wire of the prototypes tested.

The data recorded for prototype #1 during the ten actuations were collected in figure 12. The curves can be divided into three regions: the actuation, the maintenance of the structure at the maximum displacement, and finally, the recovery.

The actuation can be considered ended when the displacement starts to increase slowly, and this appended around 10% of total test time. After this point, the



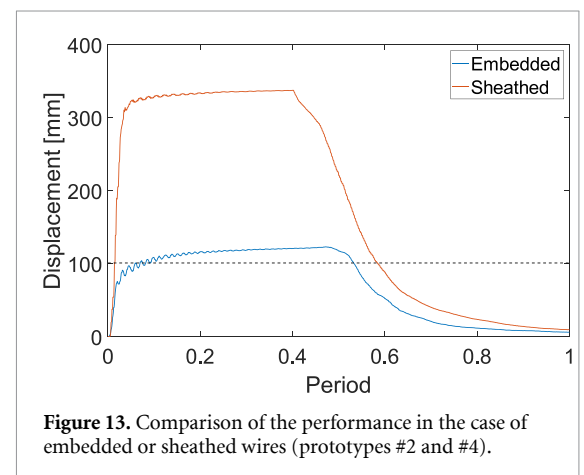
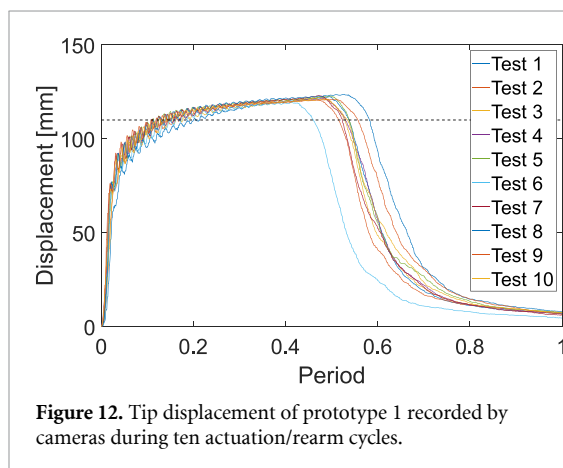
speed slows down considerably and with it also the effectiveness of the actuation. Actuation and maintenance phases together reach 50% of test period. The maximum displacement of the first prototype is about 121 mm.

The last part of the curve represents the recovery. The electrical power was turned off and, consequently, the temperature of the wire decreased, reaching the martensite start and martensite finish temperature by natural convection cooling. This produced a quite slow recovery of about the same duration of the actuation-maintaining phases together. The elasticity of the helix allowed a complete rearm of the wire. So, the structure comes back to the initial position without residual deformations and displacements. The first and the second graph's regions present some oscillations, especially near the maximum displacement and the maintenance of the prototype. These oscillations are due to the instabilities of the helix and to the natural equilibrium between the pulling action of the wire and the reaction of the structure that tends to come back to the undeformed condition.

The displacement calculated by numerical simulation was 110 mm. The analyses approximated the experimental behaviour of the structure with acceptable accuracy, underestimating it by about 8%. Experimentally the NiTi wires can transmit contraction to the composite, even if completely

**Table 6.** Summary of the average maximum displacements for each wire of the prototypes

Prototype ID	Wire	Displacement (mm)	Curvature radius (mm)	Angle of curvature (rad)
# 1	1	121.8	670.2	42.7
# 2	1	85.5	882.2	32.5
	2	82.6	894.6	32.1
# 3	1	103.0	839.9	34.1
	2	99.8	866.7	33.1
# 4	1	344.3	252.1	113.6
	2	300.5	279.3	102.6
# 5	1	168.2	502.6	57.1
	2	175.7	447.0	64.1
# 6	1	286.2	283.4	101.1
	2	308.6	256.7	111.6
	3	266.9	324.8	88.2
# 7	1	74.1	1283.6	22.3
	2	106.2	841.6	34.1
	3	122.2	775.9	37.0
	4	78.5	1142.9	25.1
	5	65.7	1322.2	21.7
	6	65.9	1405.5	20.4



incorporated. The embedding inside composite does not result in a fixing constraint and thus the wire contraction contributes to the total displacement. This phenomenon was analytically formulated in [35]. In the numerical model, instead, the wire was modelled only outside the composite structure so this contribution to the movement of the helix was omitted, but this approximation was considered admissible in the current design phase. This assumption must be reconsidered if accurate control of the boroscope tip is desired.

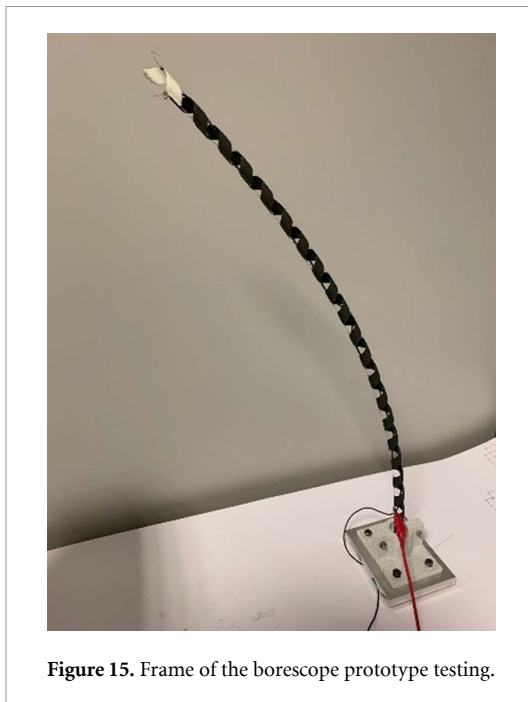
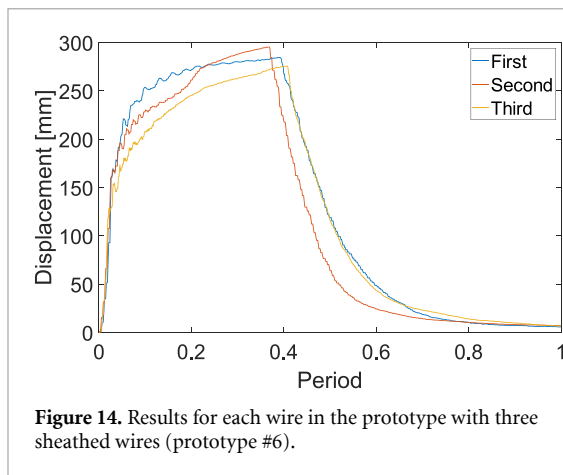
Figures 12 and 13 reported only the numerical final displacement and not the history during actuation and cooling. The actuation in numerical simulations was implemented by a linear increase in the temperature. The corresponding time in Abaqus is not comparable with the experimental one so the two curves cannot overlap. The numerical final

displacement was shown as a horizontal black dotted line, to compare it with the final displacement of the experimental tests.

Figure 13 reported the curves of the activations of two prototypes with two SMA wires, comparing the direct embedding and the use of sleeves. Even if the SMA inside the composite layers contributes to the total displacement, the wires in the sheathed structure are completely free to recover their initial shape during the heating. This allows obtaining displacement three times higher than embedded wires.

As reported in table 6, the increase of wires' pre-strain (prototypes #2 vs. #3) allows to reach a higher maximum displacement. This effect is not linear: doubling the pre-stain (6% instead of 3%) did not produce a large increase in displacement obtained.

Relevant was the test on the prototype with three wires, as this is the minimum configuration to obtain



bending in all directions. The results are reported in figure 14. The total displacement reached was slightly lower than the displacement of the previous prototype with sleeves. This difference can be linked to the higher stiffness of the structure with three wires than the one with two wires, due to the addition of one passive wire. The three curves give a similar trend, with some differences in the actuation region of the graph. These could be attributed to local effects of helix manufacturing, like a non-perfect uniformity of the structure or the presence of solid resin inside sheaths. The resin indeed, during the autoclave cycle, could partially close the section of some sleeves, hindering the movement of the wire.

Comparing prototypes with the same constraint but a different number of wires, as prototypes #6 vs. #5 and #7 vs. #2, emerged that increasing the number of wires is not beneficial for the bending performance, due to an increase of the structure stiffness. So,

the minimum number useful for accuracy should be recommended.

In table 6 are reported also the mean curvature radius and angle of each prototype testes. Prototypes #4 and #6 are the ones with higher angles, comparable or greater to the ones reported in literature. Also considering the lowest values reached, these are similar to the ones obtained for continuous backbones structures realized in different materials.

## 5. Discussion

The goal of this work was to propose a new concept for a borescope for space applications with no hinges or other mechanisms. The idea starts from continuous bioinspired robots. Some initial design constraints were set by the authors. The load-bearing structure was defined to be a continuous helical structure made of carbon fibre-reinforced composite material, while the bending motion actuators were NiTi wires. The helix length and the diameter were fixed with a pilot assessment respectively at 500 mm and 10 mm.

The preliminary design used a simplified model in which the wire action was simulated by applying force couples reproducing the contraction of the wire. Through this model some parameters were obtained to maximize lateral displacement: 25 mm helix pitch, 10 mm strip width, and composite  $[0]_4$  lamination sequence.

Using these parameters, a more refined model that simulates the transformation of NiTi wires was implemented to estimate the bending performances. The following experimental validation proved that the numerical analyses assessed the experimental results with acceptable accuracy but underestimated them systematically. The reason lies in the contribution to total contraction given by the portions of wire completely embedded within the composite. Whereas in the numerical model, the wire was modelled only outside the composite structure. This approximation was considered admissible in the current design phase, considering the numerical burden of this simulation, but it must be reconsidered if an accurate control of the borescope tip is desired.

The experimental tests on seven prototypes not only allowed to confirm this concept but also brought to the definition of some manufacturing aspects. First, the optimal number of wires to control flexion in all directions is three. This also avoids excessively increasing the structure stiffness. Second, it is advisable to slide the NiTi wires inside sleeves embedded in the composite to obtain higher performance. In this way is possible to exploit the full contraction of the wires. The drawback is that these sleeves are quite invasive on the thin composite structure. This requires an assessment of the prototype's integrity when it is loaded.

## 6. Conclusions

In conclusion, given the initial restriction of avoiding joints and reducing the weights, the chosen helix structure resulted suitable for the considered applications. The structure provided a good trade-off between compliance and stiffness. It resulted flexible enough to achieve a good degree of bending and, at the same time, sufficiently rigid to allow complete rearm of the NiTi wires when they are cooled. In this way, the use of an antagonistic actuator is not essential. Moreover, the selection of composites rather than other materials, such as metals, guarantee lightness and allowed to tailor the stiffness of the structure by varying the lamination sequence. The composite materials allow also an easy embedding of the wires during the manufacturing procedure. Finally, another advantage of the best configuration achieved among those proposed, is that it is possible to change the wires since these are inserted inside sleeves and are constrained only at the ends. Removing the clamps the wire can be pull out and changed.

The maximum displacements obtained of 340 mm and 110° of curvature for sleeve prototypes and 132 mm for prototypes with direct embedding were satisfying. The good results reached encourage further research on this structure and work, studying for example the cyclic actuation of the SMA and the fatigue life. Moreover, the initially stated constraints can be relaxed or modified, so in future applications, the introduction of joints could be considered to obtain a more complex movement of the arm.

## Data availability statement

The data cannot be made publicly available upon publication because the cost of preparing, depositing and hosting the data would be prohibitive within the terms of this research project. The data that support the findings of this study are available upon reasonable request from the authors.

## Acknowledgments

Authors would like to acknowledge gratefully ASI for the financial support under the collaboration agreement with Politecnico di Milano No. 2018-5-HH.0 of the framework Agreement No. 2016-27-H.0, aiming at designing shape memory alloy actuation systems for aerospace applications.

## ORCID iDs

Daniela Rigamonti  <https://orcid.org/0000-0002-0047-9002>

Antonio Mattia Grande  <https://orcid.org/0000-0003-4913-2525>

## References

- [1] da Veiga T, Chandler J H, Lloyd P, Pittiglio G, Wilkinson N J, Hoshiar A K, Harris R A and Valdastrì P 2020 Challenges of continuum robots in clinical context: a review *Progr. Biomed. Eng.* **2** 032003
- [2] Wang T 2020 *et al* Design and analysis of a snake-like surgical robot with continuum joints *ICARM 2020–2020 5th IEEE Int. Conf. on Advanced Robotics and Mechatronics* pp 178–83
- [3] Santiago J L C, Walker I D and Godage I S 2015 Continuum robots for space applications based on layer-jamming scales with stiffening capability *IEEE Aerospace Conf. Proc.* vol 2015 pp 1–13
- [4] Mehling J S, Diftler M A, Chu M and Valvo M 2006 A minimally invasive tendril robot for in-space inspection *Proc. 1st IEEE/RAS-EMBS Int. Conf. on Biomedical Robotics and Biomechanics, 2006, BioRob 2006* vol 2006 pp 690–5
- [5] Walker I D 2013 Continuous backbone ‘continuum’ robot manipulators *ISRN Robot.* **2013** 1–19
- [6] Kolachalama S and Lakshmanan S 2020 Continuum robots for manipulation applications: a survey *J. Robot.* **2020** 1–19
- [7] Wooten M B and Walker I D 2018 Vine-inspired continuum tendril robots and circumnutations *Robotics* **7** 58
- [8] Giorelli M, Renda F, Calisti M, Arienti A, Ferri G and Laschi C 2015 Neural network and Jacobian method for solving the inverse statics of a cable-driven soft arm with nonconstant curvature *IEEE Trans. Robot.* **31** 823–34
- [9] Frascas J, MacIas M, Noh Y and Althoefer K 2018 Fluidical bending actuator designed for soft octopus robot tentacle *2018 IEEE Int. Conf. on Soft Robotics, RoboSoft 2018 (July 2018)* pp 253–7
- [10] Yang J, Pitarch E P, Potratz J, Beck S and Abdel-Malek K 2006 Synthesis and analysis of a flexible elephant trunk robot *Adv. Robot.* **20** 631–59
- [11] Luo R, Wang T, Shi Z and Tian J 2017 Design and kinematic analysis of an elephant-trunk-like robot with shape memory alloy actuators *IEEE 2nd Advanced Information Technology, Electronic and Automation Control Conf. (IAEAC) (Chongqing, China)* pp 157–61
- [12] Kai X, Liu Z, Zhao B, Liu H and Zhu X 2019 Composed continuum mechanism for compliant mechanical postural synergy: an anthropomorphic hand design example *Mech. Mach. Theory* **132** 108–22
- [13] Rone W S and Ben-Tzvi P 2014 Continuum robotic tail loading analysis for mobile robot stabilization and maneuvering *Proc. ASME 2014 Int. Design Engineering Technical Conf. and Computers and Information in Engineering Conf. Volume 5A: 38th Mechanisms and Robotics Conference (Buffalo, New York, USA, 17–20 August 2014)*
- [14] Tadesse Y, Thayer N and Priya S 2010 Tailoring the response time of shape memory alloy wires through active cooling and pre-stress *J. Intell. Mater. Syst. Struct.* **21** 19–40
- [15] Borlandelli E, Scarselli D, Nespoli A, Rigamonti D, Bettini P, Morandini M, Villa E, Sala G and Quadrio M 2015 Design and experimental characterization of a NiTi-based, high-frequency, centripetal peristaltic actuator *Smart Mater. Struct.* **24** 035008
- [16] Auricchio F, Boatti E and Conti M 2015 Chapter 11 - SMA biomedical applications *Shape Memory Alloy Engineering* ed L Lecce and A Concilio (Butterworth-Heinemann) pp 307–41
- [17] Menna C, Auricchio F and Asprone D 2015 Applications of shape memory alloys in structural engineering (<https://doi.org/10.1016/B978-0-08-099920-3.00013-9>)
- [18] Hartl D J and Lagoudas D C 2007 Aerospace applications of shape memory alloys *Proc. Inst. Mech. Eng. G* **221** 535–52
- [19] Fischer H, Vogel B, Pflieger W and Besser H 1999 Flexible distal tip made of nitinol (NiTi) for a steerable endoscopic camera system *Mater. Sci. Eng. A* **273–5** 780–3

- [20] de Sars V, Haliyo S and Szewczyk J 2010 A practical approach to the design and control of active endoscopes *Mechatronics* **20** 251–64
- [21] Haga Y, Esashi M and Maeda S 2000 Bending, torsional and extending active catheter assembled using electroplating *Proc. IEEE Micro Electro Mechanical Systems (MEMS)* pp 181–6
- [22] Mineta T, Mitsui T, Watanabe Y, Kobayashi S, Haga Y and Esashi M 2002 An active guide wire with shape memory alloy bending actuator fabricated by room temperature process *Sens. Actuators A* **97–98** 632–7
- [23] Haga Y, Mineta T, Makishi W, Matsunaga T and Esashi M 2010 Active bending catheter and electric endoscope using shape memory alloy *Shape Memory Alloys* ed C Cismasiu (Sciyo) (<https://doi.org/10.5772/9971>)
- [24] Haga Y, Mizushima M, Matsunaga T, Totsu K and Esashi M 2005 Active bending ileus tube using shape memory alloy for treatment of intestinal obstruction *2005 3rd IEEE/EMBS Special Topic Conf. on Microtechnology in Medicine and Biology* vol 2005 pp 249–52
- [25] Hadi A, Akbari H, Tarvirdizadeh B and Alipour K 2016 Developing a novel continuum module actuated by shape memory alloys *Sens. Actuators A* **243** 90–102
- [26] Cao Y, Ju F, Zhang L, Bai D, Qi F and Chen B 2018 A novel variable-stiffness flexible manipulator actuated by shape memory alloy for minimally invasive surgery *Proc. Inst. Mech. Eng. H* **232** 1098–110
- [27] Padasdao B, Batsaikhan Z, Lafreniere S, Rabiei M and Konh B 2022 Modeling and operator control of a robotic tool for bidirectional manipulation in targeted prostate biopsy *2022 Int. Symp. on Medical Robotics, ISMR 2022* (<https://doi.org/10.1109/ISMR48347.2022.9807514>)
- [28] Sarma A *et al* 2020 Towards the development of an ultrasound-guided robotically steerable guidewire *2020 Int. Symp. on Medical Robotics, ISMR 2020* pp 173–80
- [29] Tian J, Wang T, Fang X and Shi Z 2020 Design, fabrication and modeling analysis of a spiral support structure with superelastic Ni-Ti shape memory alloy for continuum robot *Smart Mater. Struct.* **29** 045007
- [30] Sivaperuman Kalairaj M, Yeow B S, Lim C M and Ren H 2020 Nitinol actuated soft structures towards transnasal drug delivery: a pilot cadaver study *Med. Biol. Eng. Comput.* **58** 611–23
- [31] Lagoudas D C, Entchev P B and Kumar P K 2003 Thermomechanical characterization of SMA actuators under cyclic loading *Proc. of the ASME 2003 Int. Mechanical Engineering Congress and Exposition, Aerospace (Washington, DC, USA, 15–21 November 2003)* vol 42933 pp 211–7
- [32] Qidwai M A and Lagoudas D C 2000 Numerical implementation of a shape memory alloy thermomechanical constitutive model using return mapping algorithms *Int. J. Numer. Methods Eng.* **47** 1123–68
- [33] Airoidi A, Rigamonti D, Sala G, Bettini P, Villa E and Nespoli A 2021 Development of an actuated corrugated laminate for morphing structures *Aeronaut. J.* **125** 180–204
- [34] Lucas B D and Kanade T 1981 An iterative image registration technique with an application to stereo vision (IJCAI) an iterative image registration technique with an application to stereo vision (available at: [www.researchgate.net/publication/215458777](http://www.researchgate.net/publication/215458777))
- [35] Bettini P, Rigamonti D and Sala G 2021 SMA for composite aerospace structures *Shape Memory Alloy Engineering* (Elsevier) pp 561–90